INSTITUTE OF PHYSICS PUBLISHING JOURNAL OF PHYSICS B: ATOMIC, MOLECULAR AND OPTICAL PHYSICS

J. Phys. B: At. Mol. Opt. Phys. **37** (2004) 917–936 PII: S0953-4075(04)72100-8

Implementation of exterior complex scaling in B-splines to solve atomic and molecular collision problems

C William McCurdy[1,2] **and Fernando Martín**[3]

[1] Lawrence Berkeley National Laboratory, Computing Sciences, Berkeley, CA 94720, USA
[2] Department of Applied Science, University of California, Davis, Livermore, CA 95616, USA
[3] Departamento de Química C-9, Universidad Autónoma de Madrid, 28049 Madrid, Spain

E-mail: cwmccurdy@lbl.gov and fernando.martin@uam.es

Received 18 November 2003
Published 10 February 2004
Online at stacks.iop.org/JPhysB/37/917 (DOI: 10.1088/0953-4075/37/4/017)

Abstract

B-spline methods are now well established as widely applicable tools for the evaluation of atomic and molecular continuum states. The mathematical technique of exterior complex scaling has been shown, in a variety of other implementations, to be a powerful method with which to solve atomic and molecular scattering problems, because it allows the correct imposition of continuum boundary conditions without their explicit analytic application. In this paper, an implementation of exterior complex scaling in B-splines is described that can bring the well-developed technology of B-splines to bear on new problems, including multiple ionization and breakup problems, in a straightforward way. The approach is demonstrated for examples involving the continuum motion of nuclei in diatomic molecules as well as electronic continua. For problems involving electrons, a method based on Poisson's equation is presented for computing two-electron integrals over B-splines under exterior complex scaling.

1. Introduction

An important aspect of the implementation of any method involving square-integrable basis functions, such as B-splines, to solve scattering problems is the treatment of asymptotic boundary conditions. The imposition of scattering boundary conditions is always troublesome in methods involving square-integrable basis sets. One approach to this question that was explored extensively begining more than 30 years ago, and reviewed in the 1980s (Reinhardt 1982), is the method of complex scaling. In simple complex scaling the coordinates of all the particles in the Hamiltonian are scaled by a complex-valued scale factor according to $r \rightarrow r\,\mathrm{e}^{\mathrm{i}\eta}$. This idea has been successful for resonance energy calculations, but has rarely

proven useful for scattering applications in which the wavefunction is itself required at real values of the coordinates for the calculation of scattering amplitudes. However, a related idea, that of exterior complex scaling (ECS), which was also posed more than 20 years ago (Simon 1979, Nicolaides and Beck 1978), has been developed over the past decade into a powerful approach to general scattering problems using square-integrable basis set representations.

The ECS transformation that underlies this approach scales the coordinates only outside a fixed radius,

$$r \to \begin{cases} r & \text{for} \quad r \leqslant R_0 \\ R_0 + (r - R_0)\,\mathrm{e}^{\mathrm{i}\eta} & \text{for} \quad r > R_0 \end{cases} \tag{1}$$

where R_0 defines the radius within which the wavefunction will be the usual function of real-valued coordinates, and η is a scaling angle. In an exact or converged calculation the solutions of the Schrödinger equation for $r < R_0$ do not depend on η, because exterior complex scaling provides the exact solution with the coordinates taken on a particular complex contour (Simon 1979). As we will review below, setting $\eta \neq 0$ while imposing the boundary condition that *on the ECS contour* the wavefunction vanish as $r \to \infty$ effectively imposes outgoing scattering boundary conditions on the exact solution, and that is why the ECS approach provides a path to compute collision amplitudes. It is this property that makes ECS particularly useful in cases where the asymptotic boundary conditions make traditional methods difficult to apply.

Like simple complex scaling, the ECS method has been used in a variety of applications to compute resonance parameters, but it is its application to the calculation of collision cross sections that concerns us here. The ECS approach has been implemented for computing scattering amplitudes using finite elements (McCurdy *et al* 1997, McCurdy and Rescigno 1997), finite difference (Baertschy *et al* 1999) and with a combination of the discrete variable representation (DVR) and finite elements (Rescigno and McCurdy 2000). It has produced essentially exact results for electron-impact ionization of hydrogen (Rescigno *et al* 1999, Baertschy *et al* 2001), and has been implemented with pseudospectral methods (Telnov and Chu 1999, 2002) to treat multiphoton detachment in the context of Floquet theory for atoms in intense fields. ECS has also been applied directly to wave packet propagation in the time-dependent Schrödinger equation with external fields (McCurdy *et al* 1991).

A key property of all these modern implementations of the ECS method is that they involve grid-like numerical methods that are easily able to converge the calculations in question so that *there is essentially no dependence of the physical wavefunction on the scaling parameter* η. This property is in stark contrast to early implementations of complex scaling using analytic basis sets in which an optimal value of η was determined by appeals to variational behaviour (Yaris and Winkler 1978) with respect to η for a particular size of the basis set expansion.

B-spline functions have been proposed in the last decade as an alternative tool to traditional basis set expansions to provide accurate representations of both bound and continuum states. The technology and applications of B-spline methods have been reviewed widely (Saperstein and Johnson 1996, Martín 1999, Lambropoulos *et al* 2000, Bachau *et al* 2001), but a few points are worth recalling here. In contrast to Gaussians (GTO) or Slater-type orbitals (STO), which extend to infinity, B-splines are compact L^2 integrable functions defined in a finite space usually referred to as a box. In the box, a knot sequence is defined to suit the particular problem of interest. The freedom to choose this sequence is an important advantage of the approach. The knot sequence defines the extent of the individual splines, so that integrals over two B-splines are zero if the two splines are different from zero in disjoint intervals. Thus, the resulting matrices are sparse and often, but not always, banded, which is advantageous not only to avoid linear dependences in the diagonalization procedure but also in the evaluation of matrix elements. In addition, B-splines are positive definite functions, a property that leads to

matrices that are even easier to diagonalize. A very important consequence is that B-splines are able to span a large volume to any degree of completeness without encountering the numerical problems that hinder the applicability of STOs and GTOs. This point is particularly important for the use of B-splines to describe continuum states. For example, the asymptotic behaviour of continuum states can be accurately described by placing grid points at very large distances from the nuclei. The ability of B-splines to represent diffuse and continuum states has opened up new fields of application where traditional L^2 basis sets were not appropriate. Significant examples are the study of Rydberg and multiply excited states in atomic structure calculations (van der Hart *et al* 1993, Verbockhaven and Hansen 2000), and above threshold ionization in laser–atom interactions (Cormier *et al* 1993, Sánchez *et al* 1994).

The effective completeness of B-spline basis sets is also an ideal property for obtaining accurate representations of Green functions, for which the entire spectrum is needed (Bachau *et al* 2001). This advantage can be exploited, for instance, in calculations involving multichannel coupled continua or non-linear processes such as multiphoton ionization. Furthermore, during the last few years, the use of B-splines has led to a major breakthrough in the description of continuum states of molecular systems (Sánchez and Martín 1997, 1999), since they are extremely powerful in describing simultaneously the electronic and vibrational continuum including interference effects between them. Thus adapting the existing B-spline codes to include ECS will open the possibility of using these methods to investigate single and, in particular, double molecular photoionization, since previous implementations of ECS using other grid methods have not been developed for molecules. Another relevant feature for the practical implementation of exterior complex scaling is that B-splines provide a number of continuous derivatives of the solution that is controlled by the order of the B-splines. As we will see later, all these properties are ideal for exterior complex scaling calculations. Before going into specific applications to molecular systems, it is important to investigate how the ECS–B-spline approach performs in problems for which the exact solution is known. This will lead us to introduce the main modifications with respect to the standard B-spline approach in order to generalize it to the problems mentioned above.

In this paper we present an implementation of ECS using B-splines that is able to converge ECS calculations to arbitary accuracy. We will investigate the numerical robustness of the combination of ECS and B-splines for computing both scattering cross sections and resonance energies in several example systems. We will also present a numerical algorithm based on Poisson's equation for computing the two-electron integrals needed in atomic and molecular electron-scattering, and demonstrate its use in resonance and photoionization calculations.

2. Exterior complex scaling of the Schrödinger equation

Before discussing how B-splines can be adapted to exterior complex scaling of the coordinates in the Schrödinger equation, it is worth recalling the basic formulation of ECS from earlier treatments of the subject (Rescigno *et al* 1997, Kurasov *et al* 1994). In particular we should focus on the discontinuity at $r = R_0$ of the Jacobian of the ECS transformation in equation (1). The easiest way to see the origin of that discontinuity is to first examine the case of arbitrary 'smooth' exterior complex scaling where that discontinuity does not appear, which we do briefly in section 2.1, and then specialize to the present case of 'sharp' exterior scaling as we do in section 2.2. This discontinuity is the central question for the use of B-splines, or any basis or grid representation, to represent the Schrödinger equation under the ECS transformation. Addressing it correctly is the key to constructing a numerically robust implementation, and the implementation in section 3 will do so naturally.

2.1. Formulation of complex scaling for arbitrary complex coordinate contours

To begin, consider a one-dimensional radial problem for which we make a single-valued and continuous, but otherwise arbitrary, complex transformation of the coordinate r according to $r \to R(r)$. The operator, U, that performs that transformation on the wavefunction $\Psi(r)$ is defined according to

$$U\Psi(r) = J(r)\Psi(R(r)) \tag{2}$$

where the Jacobian of the transformation is

$$J(r) = \left(\frac{\mathrm{d}R(r)}{\mathrm{d}r}\right)^{1/2}. \tag{3}$$

If the original Schrödinger equation is

$$H\Psi(r) = E\Psi(r) \tag{4}$$

with

$$H = -\frac{1}{2\mu}\frac{\mathrm{d}^2}{\mathrm{d}r^2} + \frac{j(j+1)}{2\mu r^2} + V(r) \tag{5}$$

then the scaled Schrödinger equation results from a unitary transformation,

$$UHU^{-1}U\Psi = EU\Psi \tag{6}$$

in which inverse of the scaling operator is given by

$$U^{-1}\Psi = \frac{1}{J(R^{-1}(r))}\Psi(R^{-1}(r)) \tag{7}$$

and $R^{-1}(r)$ is the inverse of the function defining the complex contour.

We can represent the complex contour, $R(r)$, in the general form suggested by (Kurasov *et al* 1994),

$$R(r) = \int_0^r q(r')\,\mathrm{d}r' \tag{8}$$

so that $\mathrm{d}R(r) = q(r)\,\mathrm{d}r$ and the exterior scaling transformation is specified by requiring $q(r)$ to satisfy the conditions

$$q(r) \to \begin{cases} 1 & \text{for} \quad r \to 0 \\ \mathrm{e}^{\mathrm{i}\eta} & \text{for} \quad r \to \infty. \end{cases} \tag{9}$$

In this way we can describe both 'smooth' exterior scaling, in which $R(r)$ is continuously differentiable, and the 'sharp' exterior scaling transformation in equation (1). The transformed Schrödinger equation that results is

$$\hat{H}\phi(r) = E\phi(r) \tag{10}$$

where $\phi(r) = \Psi(R(r))$ and the transformed Hamiltonian has the form

$$\hat{H}(r) = -\frac{1}{2\mu}\left[\frac{1}{q(r)^2}\frac{\mathrm{d}^2}{\mathrm{d}r^2} - \frac{q'(r)}{q(r)^3}\frac{\mathrm{d}}{\mathrm{d}r}\right] + \frac{j(j+1)}{2\mu R(r)^2} + V(R(r)). \tag{11}$$

In a basis set expansion the idea is to expand the transformed wavefunction, $\phi(r)$, and *not* $U\Psi(r)$ appearing in equation (2) which contains the Jacobian factor $q(r)^{1/2}$, in a set of square-integrable functions $\chi_n(r)$. The derivative portion of the kinetic energy matrix elements

is therefore defined according to

$$K_{mn} = -\frac{1}{2\mu}\int_0^\infty \chi_m(r)\left[\frac{1}{q(r)^2}\frac{\mathrm{d}^2}{\mathrm{d}r^2} - \frac{q(r)'}{q(r)^3}\frac{\mathrm{d}}{\mathrm{d}r}\right]\chi_n(r)q(r)\,\mathrm{d}r \tag{12}$$

$$= \frac{1}{2\mu}\int_0^\infty \chi_m'(r)\frac{1}{q(r)}\chi_n'(r)\,\mathrm{d}r \tag{13}$$

where the second equality, which exhibits the fact that the kinetic energy matrix is complex symmetric, comes from integrating by parts and using the fact that the χ_n vanish at the extrema of the grid. The other matrix elements, where the operator is just a function of $R(r)$, are defined in the entirely obvious way, with the potential matrix elements, for example, being given by the integral

$$V_{mn} = \int_0^\infty \chi_m(r)V(R(r))\chi_n(r)q(r)\,\mathrm{d}r \tag{14}$$

with the volume element $q(r)\,\mathrm{d}r$. Thus the matrix representation of the Hamiltonian is explicitly complex symmetric for any contour defined by $q(r)$.

Now we are ready to turn to the conditions on $\phi(r)$ and its derivatives at $r = R_0$ for the case of 'sharp' exterior scaling in equation (1).

2.2. 'Sharp' exterior scaling and the question of the discontinuity of the Jacobian

To use the exterior scaling contour originally defined by equation (1), we simply set the function $q(r)$ equal to

$$q(r) = \begin{cases} 1 & \text{for} \quad r \leqslant R_0 \\ \mathrm{e}^{\mathrm{i}\theta} & \text{for} \quad r > R_0. \end{cases} \tag{15}$$

With this definition the Jacobian

$$J(r) = q(r)^{1/2} \tag{16}$$

is obviously discontinuous because $q(r)$ is discontinuous. The transformed wavefunction $\phi(r) = \Psi(R(r))$ is always continuous, although its first derivative with respect to r is not continuous because

$$\frac{\mathrm{d}}{\mathrm{d}r}\phi(r) = \frac{\mathrm{d}R(r)}{\mathrm{d}r}\Psi'(R(r)) = q(r)\Psi'(R(r)). \tag{17}$$

In every implementation of ECS using a basis set expansion it is exactly this point that is critical, because the numerical convergence properties depend on the correct representation of the wavefunction at $r = R_0$. Fortunately, as the list of successful applications of ECS attests, it is generally not difficult to treat the point R_0 correctly. For example, in the implementation in terms of the discrete variable representation and finite elements (Rescigno and McCurdy 2000), it was shown that putting a DVR finite element boundary point at R_0 and requiring only continuity of the value of the function at that point gives the DVR basis the ability to represent $\phi(r)$ with a continuous value at R_0, but with a discontinuous derivative. Other implementations describe the details differently, but accomplish the same end (Telnov and Chu 1999).

In general, basis functions of compact support such as B-splines can treat the condition at R_0 *exactly*, while complex analytic basis set expansions, such as expansions in Slater or Gaussian functions cannot. The successful use of complex analytic basis set expansions with ECS generally requires 'smooth' exterior scaling in which $q(r)$ is continuous and continuously differentiable (Karlsson 1998). B-splines, however, can treat the 'sharp' exterior scaling of equation (1) perfectly.

3. B-splines and exterior complex scaling

To see how to apply B-splines to the ECS transformation we need their definition as given, for example, by de Boor (1978). We specify a series of knots $t_i \leqslant t_{i+1}$ in the coordinate, r, and the splines of order k are defined by a recursion relation,

$$B_i^k(r) = \frac{r - t_i}{t_{i+k-1} - t_i} B_i^{k-1}(r) + \frac{t_{i+k} - r}{t_{i+k} - t_{i+1}} B_{i+1}^{k-1}(r) \tag{18}$$

together with the definition of B-splines of order $k = 1$

$$B_i^1(r) = \begin{cases} 1 & \text{for} \quad t_i \leqslant r < t_{i+1} \\ 0 & \text{otherwise.} \end{cases} \tag{19}$$

The case of $k = 2$ gives 'tent functions'. Once the recursion is taken to third order ($k = 3$) one has a set of the familiar (smooth) quadratic splines. Higher orders provide more spline functions in the basis covering successively larger numbers of knots as the order is increased. They also give more continuous derivatives as the order is increased.

The basis of B-splines is entirely defined by the knots $\{t_i\}$. These are built from a grid in the r coordinate (the breakpoint sequence ξ_i) by assigning a multiplicity to each grid point (breakpoint). Thus the positions of the breakpoints coincide with those of the knotpoints, but several knotpoints may coincide with a single breakpoint when multiplicity is larger than one. In most applications, multiple breakpoints are only used near the borders (e.g. at the origin to provide more flexibility in this region). Thus the number of knotpoints is only slightly larger than the number of breakpoints. Details of this technology have been reviewed at length elsewhere (Bachau *et al* 2001) and will not be further described.

What concerns us here is the following question. B-splines of order k have continuous derivatives up to order $k - 2$. So how can they be used to represent functions that have discontinuous derivatives? The answer is straightforward. Define the splines as $B_i^k(R(r))$. That is, put the breakpoints, ξ_i and therefore the knots, t_j on the complex exterior scaling contour, and *place one of the breakpoints and its corresponding knot at* $t_j = R_0$. Then $B_i^k(R(r))$ has a discontinuous first derivative with respect to r at $r = R_0$, because the derivative of $R(r)$ is discontinuous at that point. Furthermore, the discontinuity in the first derivative of all the B-splines that span the point R_0 can be shown to be exactly that of equation (17).

Figure 1 shows the resulting B-splines, at order $k = 8$, and demonstrates clearly that the derivatives of the B-splines are discontinuous. In the figure one sees that either the real or the imaginary part of each B-spline shows a discontinuous slope. Another interesting property of ECS B-splines is that the B-splines that do not straddle the point R_0 are real, whether they are on the complex part of the contour or not.

With the breakpoints defined on the exterior scaling contour, and with one of them coinciding with R_0, the matrix elements of the operators in the one-dimensional problems considered so far are simply sums of the corresponding integrals between breakpoints,

$$V_{mn} = \sum_l \int_{\xi_l}^{\xi_{l+1}} B_n^k(x) \left(V(x) + \frac{j(j+1)}{2\mu x^2} \right) B_m^k(x)\, \mathrm{d}x \tag{20}$$

$$S_{mn} = \sum_l \int_{\xi_l}^{\xi_{l+1}} B_n^k(x) B_m^k(x)\, \mathrm{d}x \tag{21}$$

$$K_{mn} = \frac{1}{2\mu} \sum_l \int_{\xi_l}^{\xi_{l+1}} \frac{\mathrm{d}B_n^k(x)}{\mathrm{d}x} \frac{\mathrm{d}B_m^k(x)}{\mathrm{d}x}\, \mathrm{d}x \tag{22}$$

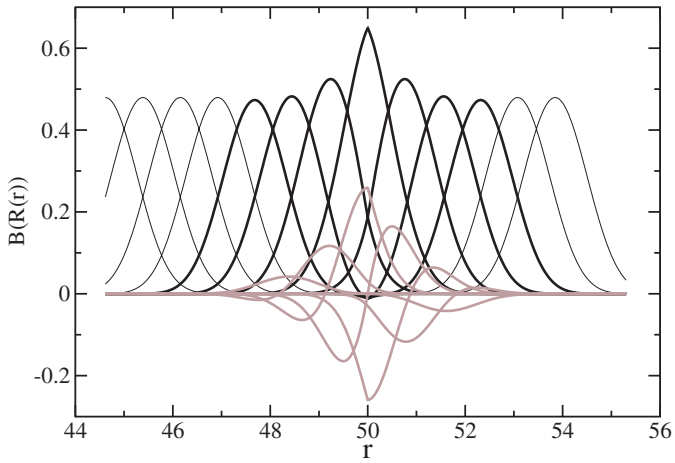

Figure 1. Eighth-order B-splines on the complex exterior scaling contour with $R_0 = 50$ and $\eta = 40^\circ$. Heavy black lines are the real parts of the only complex splines, and thin black lines are the real B-splines. Grey lines are the imaginary parts.

where $\xi_1 = 0$ and $\xi_N = R(r_{\max})$ is the end of the complex exterior scaling contour. In each interval in these sums, the integrals may be performed, for example, with simple Gauss–Legendre quadrature, but only the integrals over intervals on which both B-splines are nonzero are required. Each of the integrals appearing here is on a straight line, the ends of which may be real or complex. The Jacobian factor, $q(r)$, of the previous sections is automatically included because the limits of the integrals are explicitly complex on the complex part of the contour. With these definitions of the matrix elements, we can construct the B-spline representation of any one-electron Hamiltonian.

At this point we have shown how to represent the Hamiltonian under the ECS coordinate transformation. It is well known that this transformation renders resonance states square integrable provided that $\eta > -\arg(k_{\rm res})$, where $k_{\rm res}$ is the momentum associated with the complex resonance energy. So simply diagonalizing the Hamiltonian in this representation will yield the complex energies of resonance states. However, to complete the picture we need to describe how the B-spline ECS implementation can be used to compute scattering amplitudes in general.

4. Calculating scattering amplitudes using exterior complex scaling

It suffices here, and is clearest, to consider a one-dimensional radial example, because the generalization to higher dimensions and more particles is straightforward and has been treated elsewhere, for example by McCurdy and Rescigno (2000) and McCurdy *et al* (2001).

4.1. The case of short-range potentials

So consider a problem with Hamiltonian $H = T + V(r)$, where T is the kinetic energy operator and V is the potential. We write the scattering solution as a sum of the incoming or regular free-particle solution and a scattered wave $\psi^{\rm sc}(r)$

$$\Psi^+ = j_l(kr) + \psi^{\rm sc}(r) \tag{23}$$

which satisfies the driven Schrödinger equation

$$\left(\frac{k^2}{2\mu} - H\right)\psi^{sc}(r) = \left(H - \frac{k^2}{2\mu}\right) j_l(kr) \tag{24a}$$

$$= V(r)\, j_l(kr) \tag{24b}$$

and which we must solve with pure outgoing boundary conditions,

$$\psi^{sc}(r) \underset{r\to\infty}{\longrightarrow} A h_l^+(kr) \tag{25}$$

where $j_l(z)$ and $h_l^+(z)$ are Ricatti Bessel functions (Newton 1982).

Exterior complex scaling allows us to solve equation (24*b*) by simply constructing the matrix representation of $E - H$ in ECS B-splines, building the driving vector $\langle B_n(r)|V(r)|j_l(kr)\rangle$ and solving the resulting linear equations to give the B-spline representation of $\psi^{sc}(r)$. The B-spline basis enforces the boundary conditions that $\psi^{sc}(r)$ vanish at $r = 0$ and also at $r = r_{max}$, the maximum r in the list of B-spline breakpoints. As is now well known, these are the correct boundary conditions to produce a pure outgoing solution because on the ECS contour

$$\psi^{sc}(R(r)) \underset{r\to\infty}{\longrightarrow} A h_l^+(kR(r)) \underset{r\to\infty}{\longrightarrow} 0. \tag{26}$$

It is important to understand that this procedure formally requires that the potential satisfies

$$V(r) = 0 \qquad \text{for} \quad r \geqslant R_0 \tag{27}$$

because otherwise the Bessel function $j_l(kr)$ can cause the right-hand side of equation (24*b*) to diverge as r goes to infinity.

If $E \gg V(R_0)$, we can apply that condition on the right-hand side explicitly, and for most problems that is sufficient. In other words, if we want to solve a problem for a potential of a particular range, our basis representation of the Hamiltonian must cover that range. In the ECS procedure we must add a sufficient distance further for ψ^{sc} to effectively decay to zero. This point has been discussed at length elsewhere (Rescigno *et al* 1997), and it has been shown that even in the case of long-range potentials the procedure converges properly in the $R_0 \to \infty$ limit. Even so there are other ways to efficiently treat long-range problems with ECS, as we will see below.

Once we have the B-spline representation of $\psi^{sc}(r)$ we can compute the scattering amplitude from it using any one of the following forms of the integral expression for A,

$$A = \frac{2\mu}{k}\langle j_l(kr)|V(r)|\Psi^+(r)\rangle \tag{28a}$$

$$= \frac{2\mu}{k}\langle j_l(kr)|T - E|\psi^{sc}(r)\rangle_{R_0} \tag{28b}$$

$$= -\frac{1}{k} W(j_l(kr), \psi^{sc}(r))|_{r=R_0-\epsilon} \tag{28c}$$

where in equation (28*b*) the subscript R_0 denotes integration over the 'volume', $r \leqslant R_0$, and in equation (28*c*) $W(a, b) = a'b - b'a$ denotes the Wronskian with respect to r. This last form is of course the most efficient, involving only the evaluation of the ψ^{sc} and its derivative at a point just inside the scaling radius R_0. In multidimensional or multiparticle applications equation (28*c*) becomes a surface integral (McCurdy and Rescigno 2000, McCurdy *et al* 2001, Baertschy *et al* 2001), and provides a particularly efficient way to compute the scattering amplitudes.

4.2. The two-potential form and long-range potentials

Suppose the potential is long range so that we cannot satisfy, either practically or formally, the condition $E \gg V(R_0)$. The ECS procedure has a straightforward 'two-potential' form with which we can easily treat such a case. For example, imagine a problem in which the Hamiltonian can be written as

$$H = T + V_1 + V_2 \tag{29}$$

$$= H_1 + V_2 \tag{30}$$

where the potential V_1 is long range but for which we can solve the reference (distorted wave) problem

$$\left(\frac{k^2}{2\mu} - H_1\right)\psi_1^+ = 0 \tag{31}$$

with the correct scattering boundary conditions

$$\psi_1^+ = F_{l,k}(r) \tag{32a}$$

$$\underset{r\to\infty}{\longrightarrow} \exp(\mathrm{i}\delta)\sin(kr + \delta - l\pi/2) \tag{32b}$$

where $F_{l,k}(r)$ is the regular solution for the long-range potential and satisfies this form of the scattering boundary condition if V_1 falls off faster than $1/r^2$. We mention the necessary modification if V_1 is a Coulomb potential below.

Then we define the scattering solution of the full problem, Ψ^+ by

$$\Psi^+(r) = \psi_2^{\mathrm{sc}}(r) + \psi_1^+(r) \tag{33}$$

and solve the driven equation for its scattered part, ψ_2^{sc}

$$(E - H)\psi_2^{\mathrm{sc}}(r) = (H - E)\psi_1^+(r) \tag{34a}$$

$$= V_2(r)\psi_1^+(r). \tag{34b}$$

The ECS B-spline representation of this equation gives us a solution with pure outgoing boundary conditions

$$\psi_2^{\mathrm{sc}}(r) \underset{r\to\infty}{\longrightarrow} A_2 \mathrm{H}_{l,k}^+(r). \tag{35}$$

This equation also holds for $r = R_0$ if $V_2(R_0) = 0$ or $E \gg V_2(R_0)$, so we can solve equation (34*b*) with ECS B-splines and then evaluate the scattering amplitude

$$A_2 = \frac{2\mu}{k}\int_0^{R_0} \psi_1^+(r)(H_1 - E)\psi_2^{\mathrm{sc}}(r)\,\mathrm{d}r \tag{36}$$

$$= -\frac{1}{k} W\left(\psi_1^+, \psi_2^{\mathrm{sc}}\right)\Big|_{r=R_0-\epsilon}. \tag{37}$$

The full amplitude is then $A = \exp(\mathrm{i}\delta)\sin(\delta) + A_2$, the sum of A_2 and the amplitude for V_1.

In this way ECS can be used to solve combinations of short-range and power-law potentials using small values of R_0, but more importantly this procedure can address the problem of a short-range potential plus a Coulomb potential. In that case, $F_{l,k}(r)$ would be the regular partial wave Coulomb function, and A_2 would contain the additional phase shift due to V_2 (Taylor 1987). Aspects of this two-potential approach have been used in the electron-impact ionization problem (Baertschy *et al* 2001), and it can also be used in the context of electron-ion scattering where the incoming wave is a Coulomb function. Thus the B-spline ECS approach allows solution of the full scope of scattering problems normally treated in atomic and molecular physics.

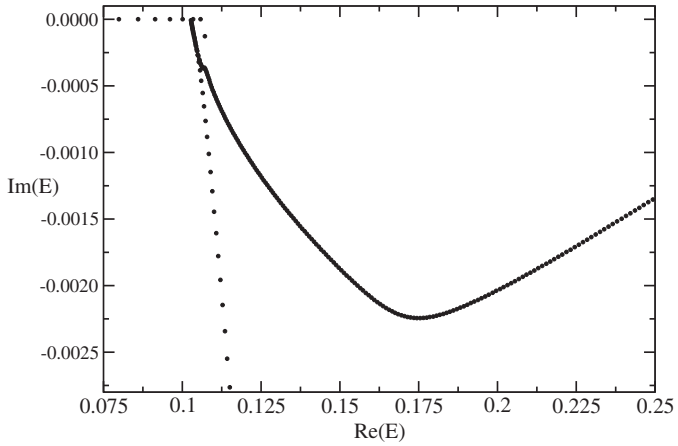

Figure 2. Spectrum for Morse potential model problem with $J = 28$. ECS parameters are $R_0 = 40$ and $\eta = 10^\circ$.

5. Numerical examples in one dimension and the convergence of the ECS B-spline representation

Although the important applications of the approach we outline in this paper will be to multiparticle, and especially many-electron, systems, it is important to establish the numerical robustness of the method. To that end we present results in this section for two simple problems, one for a mass corresponding to the reduced mass of H_2^+ and the other with the mass of the electron.

5.1. Rotational predissociation resonances for a model of H_2^+

We can make a reasonable representation for rotational predissociation of H_2^+ using a Morse potential,

$$V(r) = D_0 \left(1 - \exp\left[-\alpha(r - R_e)\right]\right)^2 \tag{38}$$

with $D_0 = 0.1026$ hartrees, $R_e = 1.9972a_0, \alpha = 0.732a_0^{-1}$ and $\mu = 918.075$. This problem provides a demonstration of the accuracy and numerical stability of the ECS B-spline representation of the Hamiltonian and also allows us to examine the typical spectrum of the discretized Hamiltonian under the ECS transformation.

Formally, the spectrum under ECS is exactly the same as under the ordinary complex dilation transformation $r \rightarrow \exp(\mathrm{i}\eta)r$. That spectrum (for a single particle) consists of discrete eigenvalues at the bound state energies (real) and resonance energies (complex poles of the S-matrix), together with a continuous spectrum beginning at zero energy ($V(r \rightarrow \infty)$) and rotated downward in the complex energy plane by an angle of -2η. Discretizations of the ECS Hamiltonian approximate this exact spectrum.

Figure 2 shows the spectrum of the ECS representation of the Hamiltonian for this model problem, with a relatively dense set of B-splines (500 B-splines on 0 to $60a_0$ with $R_0 = 40$). The spectrum in this case is similar to that of other exterior scaling implementations, in that the single, discretized, continuum cut divides into two branches. Increasing the number of spline functions on both the real and complex parts of the contour causes the spectrum to more closely approach a single discretized cut as it formally should, but that is not necessary to produce accurate results, either for the resonance eigenvalues or for the computation of

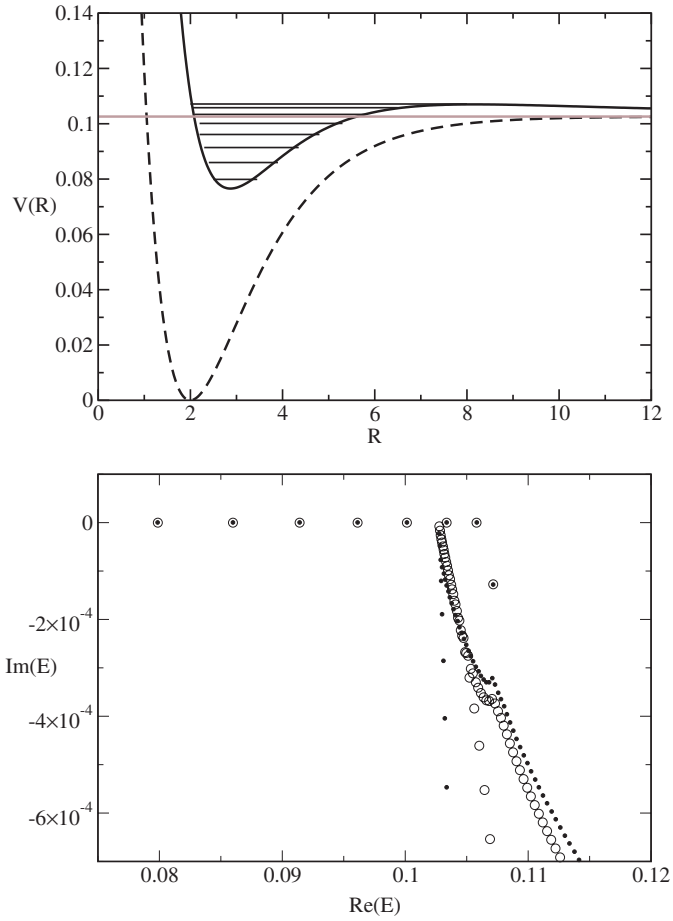

Figure 3. Upper panel: model potential for H_2^+ (dashed), its asymptotic value (grey), and the potential plus centrifugal potential for $J = 28$, showing bound states and real part of resonance energies. Lower panel: magnification of the discrete ECS spectrum for two scaling angles, $\eta = 10^\circ$ (open circles) and 30° (small closed circles).

scattering amplitudes. Scattering amplitudes may be computed accurately for energies that lie on the real energy axis in the region where the continuous spectrum is distorted in the complex energy plane by the ECS transformation. Figure 2 shows the beginning of the typical return to the real axis at high energies of the discretized spectrum for a particular basis size.

For resonances the B-spline representation gives almost perfectly stable values of $E_{\rm res} = E_R - {\rm i}\Gamma/2$ once the density of knots and the order of the B-splines are sufficient to converge the eigenvalue in question. This behaviour can be seen in figure 3 which shows a magnification of the discretized ECS spectrum for two complex scaling angles in which bound and resonant states remain immobile as the scaling angle is varied, while the discretized continuum moves further from the real axis as the angle is increased. The eigenvalues in the case of rotational angular momentum $J = 28$ are listed for two scaling angles ($\theta = 15^\circ$ and $\theta = 30^\circ$) in table 1. As is apparent in figure 3 where the levels are also indicated in the plot of the potential, there are five bound states and three resonances (one of them so narrow that it is effectively bound, one with a very long lifetime and one with a short lifetime that is essentially

Table 1. B-spline calculation of bound and resonance eigenvalues of the Morse potential for H_2^+, $R_0 = 40$ and 500 B-splines of order 8.

$\theta = 30^\circ$ E_{Real}	$\theta = 30^\circ$ E_{Imag}	$\theta = 15^\circ$ E_{Real}	$\theta = 15^\circ$ E_{Imag}
0.798 725 644(−01)	0.261 049 128(−15)	0.798 725 644(−01)	−0.547 193 893(−16)
0.859 835 519(−01)	−0.679 132 729(−16)	0.859 835 519(−01)	0.523 408 446(−16)
0.914 044 630(−01)	−0.710 553 304(−17)	0.914 044 630(−01)	0.484 728 010(−16)
0.961 248 463(−01)	−0.964 413 302(−16)	0.961 248 463(−01)	−0.165 244 533(−16)
0.100 126 858(00)	−0.122 589 060(−15)	0.100 126 858(00)	−0.104 839 538(−15)
0.103 377 844(00)	0.113 771 819(−15)	0.103 377 844(00)	0.180 566 533(−15)
0.105 805 415(00)	−0.374 162 798(−08)	0.105 805 415(00)	−0.374 138 674(−08)
0.107 148 020(00)	−0.127 834 657(−03)	0.107 147 764(00)	−0.127 676 164(−03)

at the top of the centrifugal barrier). The B-spline approach is able to converge this problem to arbitrary accuracy, but the B-spline basis used here is of the typical density used in heavy particle calculations and indicates the remarkable accuracy to be expected of this approach in practical calculations. This calculation is converged to a minimum of six significant figures.

5.2. Scattering amplitudes for the exponential potential

To demonstrate the calculation of scattering amplitudes with the ECS B-spline approach we consider the elastic scattering cross section ($\sigma = 4\pi \sin(\delta)^2/k^2$) for the exponential potential $V = -3\,\mathrm{e}^{-r}$ for elastic scattering of a particle with the mass of an electron with energy $= 1/2$ hartree. The solution of this problem is, of course, known analytically (Newton 1982), and can be computed to arbitrary accuracy in terms of Bessel functions of imaginary order. At this energy the phase shift is 2.028 859 730 528 and the cross section has the value 10.108 998 764 36. It is instructive to plot the wavefunction for this case on the complex contour from the B-spline solution of equation (24*b*). The scattered portion of the wavefunction, ψ^{sc}, is shown in figure 4 and shows how rapidly the wavefunction falls to zero beyond R_0 and how the discontinuous derivative at $r = R_0$ is represented by the ECS B-splines.

We have carried out a convergence study for a fixed value of η (40^0) and R_0 ($50a_0$) using the procedures in section 4. In figure 5 we plot the log of the relative error

$$\text{Error} = \log_{10}(|\sigma_{\text{calc}} - \sigma_{\text{exact}}|/\sigma_{\text{exact}}) \tag{39}$$

from these calculations. From examination of figure 5 two observations are obvious.

- ECS B-splines provide arbitrary precision upon increasing the order and number of spline basis functions.
- For orders higher than $k = 4$, the ECS B-spline results are monotonic functions of the number of spline basis functions.

These calculations were carried out with evenly spaced breakpoints for the ECS B-spline basis so that the comparisons for different numbers of B-spline basis functions would be systematic. Much more efficient choices of breakpoint spacings are possible as is immediately suggested by figure 4. For example, the two electron examples in the following sections made use of grids of breakpoints in which two different spacings were used: a more dense spacing for values of r up to a point slightly beyond R_0, and a sparse spacing for values on the remainder of the complex part of the ECS contour. With such a choice of the grid of breakpoints,

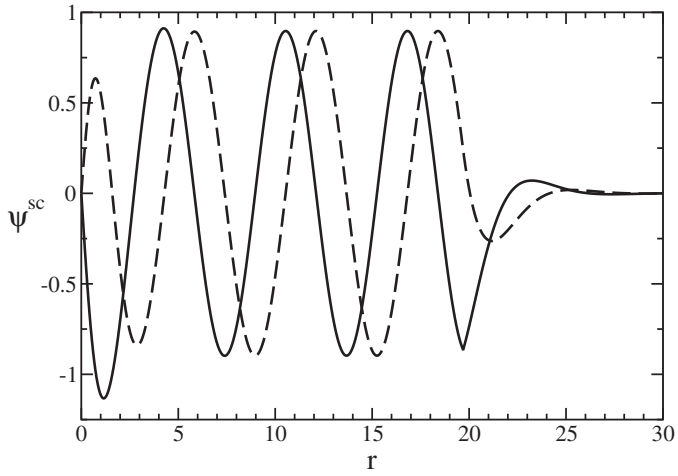

Figure 4. Wavefunction for $V = -3\exp(-r)$ at $E = 1/2$ for a unit mass from a calculation with $\eta = 40^\circ$ and $R_0 = 20a_0$, solid curve: real part, dashed: imaginary part.

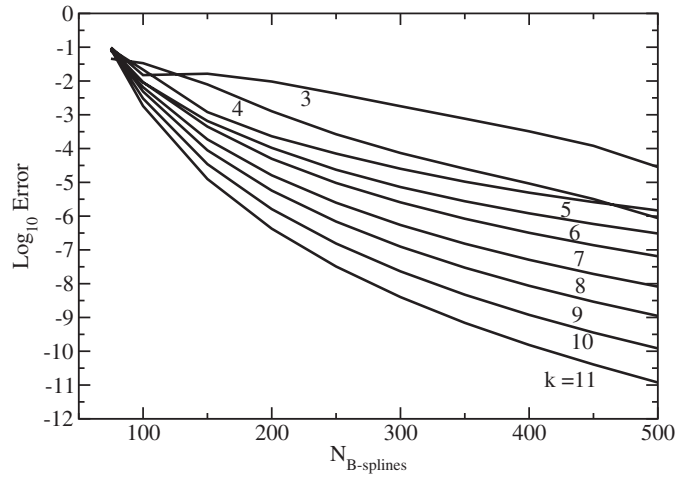

Figure 5. Relative error in cross section for the exponential potential example as a function of the number of B-splines (evenly spaced) and order k, indicated next to each curve.

100 B-splines easily provide seven or eight significant figures in the cross section for this simple example.

6. Two-electron examples

The principal motivation for this study of the ECS B-spline approach is the extension of B-spline technology to problems with more than one electron in the continuum (double photoionization and electron-impact ionization, for example). In a calculation on an atomic system, or on a molecule using a single centre expansion, the B-spline basis consists of products of radial B-splines and spherical harmonics

$$\phi_{ilm}(\mathbf{r}) = B_i^k(r)Y_{lm}(\theta, \varphi) \tag{40}$$

The preceding sections allow us to define a piecewise linear contour in the complex plane by means of defining the breakpoints of a basis of B-splines on that contour. Thus all the one-electron integrals in an atomic or molecular electron scattering calculation can be cast in the form of equations (20)–(22) and can be computed to arbitrary accuracy by performing the integration between the breakpoints using ordinary Gauss–Legendre quadrature. But to perform calculations on many-electron systems we need an efficient and accurate way to compute two-electron integrals involving B-splines on the ECS contour. Before giving some preliminary results on single photoionization and autoionizing states of helium, we now turn to the evaluation of those two-electron integrals. The approach we take is a version of the method used to compute these integrals in the discrete variable representation (McCurdy and Rescigno 2000, Rescigno and McCurdy 2000) and is similar in spirit but very different in detail to more standard approaches to the computation of these integrals in a B-spline basis (Fisher and Guo 1990, 1992, Qui and Fisher 1999).

6.1. Two-electron integrals with complex B-splines on the exterior scaling contour

In a calculation making use of a single centre basis, the two-electron integrals are of the form

$$\left\langle \phi_{i_1 l_1 m_1}(\mathbf{r_1})\phi_{i_2 l_2 m_2}(\mathbf{r_2})\right| \frac{1}{|\mathbf{r}_1 - \mathbf{r}_2|} \left|\phi_{i_3 l_3 m_3}(\mathbf{r_1})\phi_{i_4 l_4 m_4}(\mathbf{r_2})\right\rangle \tag{41}$$

and are evaluated by making a multipole expansion of the interelectron repulsion

$$\frac{1}{|\mathbf{r}_1 - \mathbf{r}_2|} = \sum_l \frac{r_<^l}{r_>^{l+1}} P_l(\cos\theta_{12}). \tag{42}$$

The angular parts of each integral can be done analytically, reducing the problem to the evaluation of radial integrals. The generic radial integral that results in each case has the form

$$\langle \rho_B | \frac{r_<^l}{r_>^{l+1}} | \rho_A \rangle = \int_0^{r\max} \mathrm{d}r \int_0^{r\max} \mathrm{d}r' \rho_B(r) \frac{r_<^l}{r_>^{l+1}} \rho_A(r') \tag{43}$$

where the densities $\rho_A(r)$ and $\rho_B(r)$ are products of B-splines, for example,

$$\rho_A(r) = B_{i_1}(r) B_{i_3}(r) \tag{44}$$

or, depending on the organization of the calculation, are sums of such terms. In this section we drop the index k for the order of the B-splines since they are all of the same order in these calculations.

The integrations in equation (43) cannot be performed easily by simple two-dimensional quadrature because the operator in r' depends on r or vice versa. To reduce this integral to simple quadratures between the B-spline breakpoints we first define the function $y(r)$

$$y(r) = r \int_0^{r\max} \rho_A(r') \frac{r_<^l}{r_>^{l+1}} \mathrm{d}r' \tag{45a}$$

$$= \int_0^r \rho_A(t) \left(\frac{t}{r}\right)^l \mathrm{d}t + \int_r^{r\max} \rho_A(t) \left(\frac{r}{t}\right)^{l+1} \mathrm{d}t \tag{45b}$$

so that the original integral can be written as a simple quadrature

$$\langle \rho_B | \frac{r_<^l}{r_>^{l+1}} | \rho_A \rangle = \int_0^{r\max} \rho_B(r) \frac{1}{r} y(r)\, \mathrm{d}r. \tag{45c}$$

Differentiation of $y(r)$ with respect to r shows that it satisfies the radial form of Poisson's equation

$$\left(\frac{\mathrm{d}^2}{\mathrm{d}r^2} - \frac{l(l+1)}{r^2}\right) y(r) = -\frac{2l+1}{r} \rho_A(r) \tag{46}$$

with the boundary conditions

$$y(0) = 0 \tag{47}$$

$$y(r_{\max}) = \frac{1}{r_{\max}^{l}} \int_0^{r_{\max}} \rho_A(t) t^l \, \mathrm{d}t. \tag{48}$$

The central idea now is to solve this equation by expanding $y(r)$ in the same basis of B-splines with which we are solving the Schrödinger equation. However, our basis of B-splines satisfies only the first of these boundary conditions. It is useful to recall (Jackson 1975) that the radial Green's function for Poisson's equation satisfies

$$\left(\frac{\mathrm{d}^2}{\mathrm{d}r^2} - \frac{l(l+1)}{r^2} \right) r g(r, r') = -\frac{2l+1}{r} \delta(r - r') \tag{49}$$

and that on the interval $(0, b)$ that Green's function (for two-point boundary conditions) is

$$g(r, r') = \frac{r_<^l}{r_>^{l+1}} - \frac{r^l r'^l}{b^{2l+1}}. \tag{50}$$

The second term in this Green's function suggests the method we will use to solve equation (46).

First we seek a solution for $y(r)$ that satisfies the boundary conditions $y(0) = 0$, but that in place of the correct boundary condition at $r_{\max}$ satisfies $y(r_{\max}) = 0$. We expand that solution in the basis of B-splines, which satisfy the boundary conditions that they vanish at 0 and $r_{\max}$,

$$y^{(0)}(r) = \sum_{i=1}^{M} C_i B_i(r). \tag{51}$$

Substituting this expansion in equation (46), multiplying by one of the B-splines from the left and integrating over r gives a matrix equation for the coefficients C_i.

$$\sum_{i=0}^{M} T_{j,i} C_i = (2l+1) U_j^A \tag{52}$$

where

$$T_{j,i} = -\int_0^{r_{\max}} B_j(r) \left(\frac{\mathrm{d}^2}{\mathrm{d}r^2} - \frac{l(l+1)}{r^2} \right) B_i(r) \, \mathrm{d}r \tag{53}$$

and

$$U_j^A = \int_0^{r_{\max}} B_j(r) \frac{1}{r} \rho_A(r) \, \mathrm{d}r. \tag{54}$$

Equation (52) has the solution

$$C_i = (2l+1) \sum_{j=1}^{M} T_{i,j}^{-1} U_j^A \tag{55}$$

and so gives us the function $y^{(0)}(r)$. To obtain a solution of Poisson's equation that has the proper boundary conditions we add a term which is a solution of the homogeneous equation corresponding to equation (46). The term we add is an exact homogeneous solution, and is analogous to the second term in Green's function in equations (49) and (50)

$$y(r) = y^{(0)}(r) + \frac{r^{l+1}}{r_{\max}^{2l+1}} \int_0^{r_{\max}} \rho_A(r') r'^l \, \mathrm{d}r' \tag{56a}$$

$$= (2l+1) \sum_{i=1}^{M} B_i(r) \sum_{j=1}^{M} T_{i,j}^{-1} U_j^A + \frac{r^{l+1}}{r_{\max}^{2l+1}} \int_0^{r_{\max}} \rho_A(r') r'^l \, \mathrm{d}r'. \tag{56b}$$

Now that we have a solution for $y(r)$ satisfying the correct boundary conditions in equation (48), we can substitute it back into the original expression for the two-electron integral, equation (45c), to obtain the final expression for the two-electron integral,

$$\langle \rho_B | \frac{r_<^l}{r_>^{l+1}} | \rho_A \rangle = (2l+1) \sum_{i,j=1}^{M} U_i^B T_{i,j}^{-1} U_j^A + \frac{1}{r_{\max}^{2l+1}} Q_l^A Q_l^B \tag{57}$$

where

$$U_j^A = \int_0^{r\max} B_j(r) \frac{1}{r} \rho_A(r)\, \mathrm{d}r \tag{58}$$

$$U_j^B = \int_0^{r\max} B_j(r) \frac{1}{r} \rho_B(r)\, \mathrm{d}r \tag{59}$$

and

$$Q_l^A = \int_0^{r\max} \rho_A(t) t^l\, \mathrm{d}t \tag{60}$$

$$Q_l^B = \int_0^{r\max} \rho_B(t) t^l\, \mathrm{d}t. \tag{61}$$

In a calculation on an atomic or molecular system in B-splines we will generally have the densities $\rho(r)$ as products of sums of B-splines, so all the quantities in equation (57) are calculated from quadratures involving B-splines.

To use equation (57) with exterior complex scaling is perfectly straightforward. All the terms appearing in that equation can be written as quadratures on intervals determined by the values of the breakpoints ξ_i of the B-splines. The matrix $T_{i,j}$ is just two times the radial kinetic energy and can be calculated using the generalization of equation (22)

$$T_{i,j} = \sum_{k=1}^{N-1} \int_{\xi_k}^{\xi_{k+1}} \frac{\mathrm{d}B_n(x)}{\mathrm{d}x} \frac{\mathrm{d}B_m(x)}{\mathrm{d}x}\, \mathrm{d}x + \sum_{l=1}^{N-1} \int_{\xi_k}^{\xi_{k+1}} B_n(x) \frac{l(l+1)}{x^2} B_m(x)\, \mathrm{d}x. \tag{62}$$

This expression can be calculated for real or complex breakpoints ξ_m as described above.

The other four factors appearing in equation (57) U_j^A, U_j^B, Q_l^A and Q_l^B can be calculated on the exterior scaling contour exactly like the one-electron potential energy matrix elements in equation (20). For example, we can evaluate

$$U_j^A = \sum_{k=1}^{N-1} \int_{\xi_k}^{\xi_{k+1}} B_j(x) \frac{1}{x} \rho_A(x)\, \mathrm{d}x \tag{63}$$

with either real or complex breakpoints.

In this approach the working expression for the two-electron radial integral, equation (57) relies on the accuracy of the underlying B-spline representation to provide an accurate value for the function $y(r)$. The other terms (the U and Q factors) can be quadratured to arbitrary accuracy.

6.2. Photoionization of helium

The total photoionization cross section of helium has been obtained from the formula

$$\sigma(\omega) = \frac{4\pi}{c\omega} \mathrm{Im} \langle \Psi_0 | \vec{\epsilon} \cdot \vec{\mu} | \Phi^{(+)} \rangle \tag{64}$$

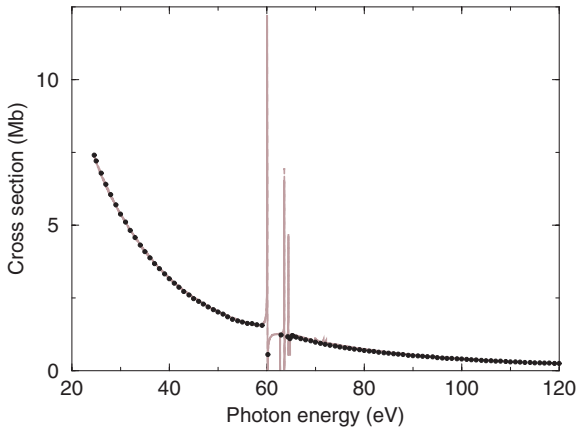

Figure 6. Helium photoionization cross section as a function of photon energy. Full curve: present results (length gauge); dashed curve (velocity gauge); circles: experimental results of Samson *et al* (1994).

where ω is the photon frequency, Ψ_0 is the ground state of helium, $\vec{\epsilon}$ is the photon polarization vector, $\vec{\mu}$ is the dipole operator and $\Phi^{(+)}$ is the outgoing solution of the driven Schrödinger equation for one-photon absorption:

$$(E_0 + \hbar\omega - H)\Phi^{(+)} = \vec{\epsilon} \cdot \vec{\mu}\Psi_0 \tag{65}$$

where E_0 is the ground state energy. The latter equation has been solved in a basis of 4800 two-electron configurations built from all possible products of one-electron orbitals with $l = 0$–3 that result from diagonalization of the He^+ Hamiltonian in a basis of eighth-order B-splines defined in a box of 60 au. The ECS parameters are $R_0 = 24$ au and $\theta = 30°$. In this case, a bilinear sequence has been used: 34 B-splines in the interval $0 \leqslant r \leqslant 30$ au and six in the interval $30 < r \leqslant 60$ au. The ground state appearing in equation (65) was represented in a basis of 100 two-electron configurations built from products of STOs as defined by Tweed (1972). The STOs were expanded in the same B-spline basis as that used for He^+ orbitals. Only STOs with $l = 0$–3 have been considered. In spite of the modest size of the STO configuration basis, the calculated ground state energy, $E_0 = -2.902\,2583$ au, is close to the experimental value $E_0 = -2.903\,7179$ au (Hart and Herzberg 1957).

In figure 6, we show the calculated photoionization spectrum. It can be seen that results obtained in the length and velocity gauges are indistinguishable, which is an indication of the practical completeness of the B-spline basis set. The photoionization spectrum exhibits helium resonances with the well-known Fano profiles. For comparison, figure 6 also includes the high precision measurements of Samson *et al* (1994) whose accuracy ranges from 1 to 2%. The comparison is made on an absolute scale. The agreement between theory and experiment is excellent in the whole energy range, except in the vicinity of the resonance peaks due to the limited energy resolution of the experiment. This agreement is also very good in the region where the double ionization continuum is open.

We have evaluated the energy positions and autoionization widths of the observed resonances. This information arises naturally by diagonalizing H in the complex plane (see the previous section) using the same B-spline basis as that used to solve equation (65). We should note in passing that the resonance parameters could also be deduced, although with greater effort, by fitting the resonance features in the photoionization cross section in figure 6. Table 2 shows a comparison between our calculated resonance parameters and the accurate

Table 2. Resonance energies and autoionization half-widths of the helium doubly excited states converging to the $N = 2$, $N = 3$ and $N = 4$ ionization thresholds. The results are compared with those obtained by Ho (Ho 1982, 1991a, 1991b). Resonances converging to the $N = 2$ threshold are labelled using the notation introduced by Cooper *et al* (1963). Resonances converging to higher thresholds are labelled using the notation $KTNn$ introduced by Herrick and Sinanoglu (1975) where K and T are quantum numbers associated with specific properties of electron correlation, N is the principal quantum number of the inner electron (i.e. it indicates the ionization threshold to which the resonance series converges) and n is the principal quantum number of the outer electron.

$2lnl'$	E (au)		$\Gamma/2$ (au)	
State	This work	(Ho 1991a)	This work	(Ho 1991a)
$2s2p_+$	−0.692 8131	−0.693 1349	0.6862(−3)	0.6866(−3)
$2s3p_-$	−0.597 0714	−0.597 0738	0.1926(−5)	0.193(−5)
$2s3p_+$	−0.564 0247	−0.564 085	0.1505(−3)	0.151(−3)
2p3d	−0.547 0199	−0.547 0927	0.4251(−7)	0.8(−8)
$2s4p_-$	−0.546 4558	−0.546 4933	0.9684(−6)	0.103(−5)
$2s4p_+$	−0.534 3360	−0.534 361	0.6563(−4)	0.65(−4)
2s4d	−0.527 5421	−0.527 6103		
$3lnl'$	E (au)		$\Gamma/2$ (au)	
State	This work	(Ho 1991b)	This work	(Ho 1991b)
1133	−0.335 6034	−0.335 6259	0.3526(−2)	0.3512(−2)
2034	−0.285 9481	−0.285 950 74	0.1705(−4)	0.1705(−4)
−1133	−0.282 6287	−0.282 828 97	0.7469(−3)	0.731 04(−3)
1134	−0.271 1684	−0.271 1933	0.1452(−2)	0.144 80(−2)
0034	−0.267 4775	−0.267 644 00	0.1076(−4)	0.113 40(−4)
2035	−0.257 4233	−0.257 4323	0.1418(−4)	0.109(−4)
−1134	−0.251 4327	−0.251 579	0.2628(−3)	0.260(−3)
$4lnl'$	E (au)		$\Gamma/2$ (au)	
State	This work	(Ho 1982)	This work	(Ho 1982)
2144	−0.194 4158	−0.194 54	0.1817(−2)	0.18(−2)
0144	−0.175 2821	−0.178 82	0.2680(−2)	0.24(−2)
3045	−0.168 8240	−0.168 85	0.2480(−4)	0.25(−2)
2145	−0.161 1404	−0.161 27	0.1083(−2)	0.41(−2)
1045	−0.159 9145	−0.1607	0.7350(−4)	0.5(−4)

values reported by Ho (Ho 1982, 1991a, 1991b), who has performed specific calculations for each resonance state. Results for resonances converging to the $N = 2$, $N = 3$ and $N = 4$ thresholds are given.

Taking into account the small value of R_0 used in the present calculations ($R_0 = 24$ au), the agreement is remarkably good. Obviously the agreement deteriorates for very diffuse resonances (the highest eigenvalues in each series), but this could be easily solved by increasing the value of R_0 and the number of l. The most significant discrepancy appears for the position of the lowest resonance $2s2p_+$. However, our calculated value is very close to that obtained in most previous calculations, which is around −0.6928 au (see, e.g., Oza 1986, Moccia and Spizzo 1987).

7. Conclusion

In this paper we have presented a practical implementation of the exterior complex scaling method with complex B-spline functions. Complex B-splines can be easily constructed using

a trivial extension of numerical algorithms and computer programs already available for real B-splines (de Boor 1978, Bachau *et al* 2001). Thus, ECS can benefit from the practical completeness of B-spline basis sets to provide almost exact results like those previously obtained with ECS using DVR or numerical methods. In contrast to the latter, B-splines allow one to work with true basis set expansions and orbitals, which is of great interest to reduce the size of a problem by discarding those orbitals and configurations that are irrelevant for the physics of the problem (a good illustration is the method used in this work to evaluate the ground state of helium).

The practical completeness of real B-splines to describe continuum states in atoms and molecules remains intact for complex B-splines. In particular, the discontinuity of the first derivative of the ECS wavefunction is exactly reproduced by the complex B-splines, which is not the case of standard basis sets such as STOs or GTOs. The latter point has been illustrated by several one-particle examples in one dimension. Extension of this idea to systems with two or more electrons has required further efforts since available algorithms to compute two-electron integrals with real B-splines cannot be used with complex B-splines. We have presented a new algorithm that allows one to evaluate these integrals to any desired accuracy. It has been successfully applied to obtain total photoionization cross sections of helium as well as energy positions and widths of the resonance peaks observed in the photoionization spectrum.

Because an extensive technology of B-spline methods already exists for applications in atomic and molecular physics, the algorithms and results presented here open the door to the application of the ECS B-spline method to problems with two electrons in the continuum, such as the double photoionization of atoms and diatomic molecules.

Acknowledgments

The work of CWM was supported by the US DOE Office of Basic Energy Sciences, Division of Chemical Sciences, and at the University of California was performed under contract DE-AC03-76SF00098. The work of FM was supported by the *Dirección General de Investigación* (Spain), projects no BFM2000-0033 and BQU2001-0147, and the European COST action D26/0002/02. CWM gratefully acknowledges a grant from the *Ministerio de Educación, Cultura y Deporte* (Spain) for a sabbatical research visit to the Universidad Autónoma de Madrid. We thank T N Rescigno for helpful discussions regarding the two-electron integrals.

References

Bachau H, Cormier E, Decleva P, Hansen J E and Martín F 2001 *Rep. Prog. Phys.* **64** 1815
Baertschy M, Rescigno T N, Isaacs W A and McCurdy C W 1999 *Phys. Rev.* A **60** R13
Baertschy M, Rescigno T N and McCurdy C W 2001 *Phys. Rev.* A **64** 022702
Cooper J W, Fano U and Prats F 1963 *Phys. Rev. Lett.* **10** 518
Cormier E, Bachau H and Zhang J 1993 *J. Phys. B: At. Mol. Opt. Phys.* **26** 4449
de Boor C 1978 *A Practical Guide to Splines* (New York: Springer)
Fisher C F and Guo W 1990 *J. Comput. Phys.* **90** 486
Fisher C F and Guo W 1992 *Int. J. Quantum Chem.* **42** 849
Hart J F and Herzberg G 1957 *Phys. Rev.* **106** 79
Herrick D R and Sinanoglu O 1975 *Phys. Rev.* A **11** 97
Ho Y K 1982 *J. Phys. B: At. Mol. Phys.* **15** L691
Ho Y K 1991a *Z. Phys.* D **21** 191
Ho Y K 1991b *Phys. Rev.* A **44** 4154
Jackson J D 1975 *Classical Electrodynamics* (New York: Wiley) p 110ff
Karlsson H O 1998 *J. Chem. Phys.* **108** 3849

Kurasov P B, Scrinzi A and Elander N 1994 *Phys. Rev.* A **49** 5095
Lambropoulos P, Maragakis P and Zhang J 2000 *Phys. Rep.* **305** 203
Martín F 1999 *J. Phys. B: At. Mol. Opt. Phys.* **32** R197
McCurdy C W, Horner D A and Rescigno T N 2001 *Phys. Rev.* A **63** 022711
McCurdy C W and Rescigno T N 1997 *Phys. Rev.* A **56** R4369
McCurdy C W and Rescigno T N 2000 *Phys. Rev.* A **62** 032712
McCurdy C W, Rescigno T N and Byrum D 1997 *Phys. Rev.* A **56** 1958
McCurdy C W, Stroud C K and Wisinski M K 1991 *Phys. Rev.* A **43** 5980
Moccia R and Spizzo P 1987 *J. Phys. B: At. Mol. Phys.* **20** 1423
Newton R G 1982 *Scattering Theory of Waves and Particles* (New York: Springer) pp 38–9
Nicolaides C A and Beck D R 1978 *Phys. Lett.* A **65** 11
Oza D H 1986 *Phys. Rev.* A **33** 824
Qui Y and Fisher C F 1999 *J. Comput. Phys.* **156** 257
Reinhardt W 1982 *Annu. Rev. Phys. Chem.* **33** 223
Rescigno T N, Baertschy M, Byrum D and McCurdy C W 1997 *Phys. Rev.* A **55** 4253
Rescigno T N, Baertschy M, Isaacs W A and McCurdy C W 1999 *Science* **286** 2474
Rescigno T N and McCurdy C W 2000 *Phys. Rev.* A **62** 032706
Samson J A R, He Z X, Yin L and Haddad G N 1994 *J. Phys. B: At. Mol. Opt. Phys.* **27** 887
Sánchez I, Cormier E, Bachau H and Zhang J 1994 *J. Phys. B: At. Mol. Opt. Phys.* **27** 4909
Sánchez I and Martín F 1997 *Phys. Rev. Lett.* **79** 1654
Sánchez I and Martín F 1999 *Phys. Rev. Lett.* **82** 3775
Saperstein J and Johnson W R 1996 *J. Phys. B: At. Mol. Opt. Phys.* **29** 5213
Simon B 1979 *Phys. Lett.* **71** 211
Taylor J R 1987 *Scattering Theory: The Quantum Theory of Nonrelativistic Collisions* (Malabar, FL: Krieger) p 266ff
Telnov D A and Chu S I 1999 *Phys. Rev.* A **59** 2864
Telnov D A and Chu S I 2002 *Phys. Rev.* A **66** 043417
Tweed R J 1972 *J. Phys. B: At. Mol. Phys.* **5** 810
van der Hart H W, Laughlin C and Hansen J E 1993 *Phys. Rev. Lett.* **71** 1506
Verbockhaven G and Hansen J E 2000 *Phys. Rev. Lett.* **84** 2810
Yaris R and Winkler P 1978 *J. Phys. B: At. Mol. Phys.* **11** 1475